Cluster coarsening and luminescence emission intensity of Ge nanoclusters in SiO 2 layers

J. M. J. Lopes, F. C. Zawislak, M. Behar, P. F. P. Fichtner, L. Rebohle, and W. Skorupa

Citation: Journal of Applied Physics **94**, 6059 (2003); doi: 10.1063/1.1616995
View online: http://dx.doi.org/10.1063/1.1616995
View Table of Contents: http://scitation.aip.org/content/aip/journal/jap/94/9?ver=pdfcov
Published by the AIP Publishing

Cluster coarsening and luminescence emission intensity of Ge nanoclusters in SiO_2 layers

J. M. J. Lopes, F. C. Zawislak,[a] and M. Behar
Instituto de Física–UFRGS, Caixa Postal 15051, 91501-970 Porto Alegre, Brazil

P. F. P. Fichtner
Departamento de Metalurgia, Escola de Engenharia–UFRGS, Porto Alegre, Brazil

L. Rebohle
Nanoparc GmbH, D-01454 Dresden, Germany

W. Skorupa
Forschungszentrum Rossendorf eV, 01314 Dresden, Germany

(Received 27 June 2003; accepted 12 August 2003)

SiO_2 layers 180 nm thick are implanted with 120 keV Ge^+ ions at a fluence of $1.2\times10^{16}\,cm^{-2}$. The distribution and coarsening evolution of Ge nanoclusters are characterized by Rutherford backscattering spectrometry and transmission electron microscopy and the results are correlated with photoluminescence measurements as a function of the annealing temperatures in the $400\,°C \leqslant T \leqslant 900\,°C$ range. At 400 °C we observe a monomodal array of clusters characterized by a mean diameter $\langle\phi\rangle=2.2$ nm which increases to $\langle\phi\rangle=5.6$ nm at 900 °C. This coarsening evolution occurs concomitantly with a small change of the total cluster–matrix interface area and an increase of the Ge content trapped in observable nanoclusters. However, at 900 °C a significant fraction of up to about 20% of the Ge content still remains distributed in the matrix around the nanoparticles. The results are discussed in terms of possible atomic mechanisms involved in the coarsening behavior that lead to the formation of the oxygen deficiency luminescence centers. © *2003 American Institute of Physics.* [DOI: 10.1063/1.1616995]

I. INTRODUCTION

Because of its notable mechanical, chemical and electric properties, silicon is the dominant material in the current technology of microelectronic devices. However, the indirect band gap makes Si a poor light emitter and consequently unsuitable for optoeletronic application. Light-emitting devices using compound semiconductors are produced, but their integrability with silicon technology is difficult and so far this has prevented satisfactory development of Si-based optoelectronic devices.

Since the discovery of intense visible light emission in porous Si,[1] a significant amount of effort has been dedicated to the production of nanostructured Si-based systems.[2–4] The formation of nanoparticles by ion implantation of semiconductor elements in SiO_2 layers thermally grown on crystalline Si is an alternative of special interest because of its compatibility with Si technology in the fabrication process. Several studies have used ion implantation of group IV elements in SiO_2 and heat treatment to obtain nanostructures that exhibit photoluminescence (PL). Red or infrared PL of Si-implanted oxides with post-annealing at diverse temperatures has been reported by various authors.[5–8] Recently Fernandez *et al.*[8] have shown a correlation between the PL emission and the mean size and density of Si nanocrystals embedded in SiO_2, suggesting that the mechanism of emission is a fundamental transition located at the $Si–SiO_2$ interface assisted by local Si–O vibration. In other studies, where visible and ultraviolet (UV) PL from Si-, Ge- and Sn-implanted silicon oxide is obtained there is general agreement that emission is caused by oxygen deficiency centers (ODCs) created during the implantation and annealing processes.[9–13] In Ge-implanted SiO_2 layers the formation of Ge nanoparticles was observed upon high thermal annealing, and strong PL in the blue–violet region was achieved, with the values of excitation and emission energy being independent of the annealing temperature and consequently of the cluster mean size.[13] These results led the authors to exclude quantum confinement effects in Ge nanoclusters and suggest that the PL emission is due to radiative transitions of ODCs located in the interfacial region between the clusters and the oxide matrix. However, concrete understanding of the formation of the PL-emitter structure that involves nanoclusters and ODCs is still being debated.

In the present work, the formation and coarsening behavior of Ge nanoclusters in SiO_2 are investigated using a combination of Rutherford backscattering spectrometry (RBS) and transmission electron microscopy (TEM). Using this combination of techniques, in addition to thermal evolution of the nanoparticle size and depth distributions, we were also able to estimate the fraction of Ge concentration not contained in large clusters and evolution of the total cluster–matrix interface area. The results obtained are correlated with the intensity of the PL emission and discussed in terms of more specific features of the microstructure evolution,

[a]Author to whom correspondence should be addressed; electronic mail: zawislak@if.ufrgs.br

thus providing insight into the atomic mechanism involved in the formation of luminescence centers.

II. EXPERIMENT

SiO_2 films 180 nm thick were thermally grown on (100) *n*-type Si substrates in wet ambient at 1000 °C. These films were implanted at room temperature (RT) with 120 keV Ge^+ ions and fluence of $1.2\times10^{16}\,cm^{-2}$ corresponding to a Gaussian-like Ge concentration-depth profile with peak concentration of about 3 at. % formed at depth of ≈100 nm below the sample surface. After implantation, pieces from the above samples were thermally annealed under N_2 flux at temperatures from 400 to 900 °C for 30 min. The concentration-depth distribution profiles of the Ge atoms before and after heat treatment were determined by RBS using a 800 keV α-particle beam. The α particles were detected by a surface barrier detector 170° with respect to the beam direction. The overall detector and electronic resolution was better than 12 keV.

The size and depth distribution of the Ge nanoclusters were obtained from cross-sectional and plan-view TEM observations using a JEM 2010 microscope from CME-UFRGS operating at 200 kV. The cross-sectional samples were prepared by ion milling and the plan-view ones by etching the Si substrate (mechanically dimpled to a few μm thin layer) using KOH solution at 60 °C for 2 h. We want to remark that, in spite of its much lower etching rate compared with pure Si, a fraction of about 20%–30%, of the SiO_2 layer could be removed if exposed to KOH solution during the time required to remove the pure Si substrate. Therefore, in order to avoid removal of the SiO_2 layer from the surface and consequently the implanted Ge content, the sample surface was glued in a glass support. In this way the SiO_2 surface was protected against direct exposure to KOH, thus only resulting in a negligible loss of SiO_2 near the SiO_2/Si interface as a consequence of exposure to KOH solution for a short time (less than about 5 min) after removal of the Si substrate.

Finally, PL and PL excitation (PLE) measurements were performed at RT in a Spex Fluoromax spectrometer with a R298 Hamamatsu photomultiplier. All spectra were corrected for the Xe lamp spectrum, photomultiplier sensitivity and interference effects.

III. RESULTS

A. Photoluminescence measurements

Figure 1 shows PL spectra of Ge-implanted SiO_2 films at different annealing temperatures under 5.17 eV excitation. The spectra consist of UV and blue–violet emission peaks around 4.25 and 3.2 eV, respectively. The PL intensity of both peaks increases with the annealing temperature whereas their relative intensity ratio only increases slightly. Maximum PL intensity of the blue–violet peak was reached at 900 °C, approximately 12 times higher than that at 400 °C. The emission energy and the full width half maximum (FWHM) of the two bands do not change significantly with the temperature or with the nanocluster mean size increase. The PLE spectra are shown in Fig. 2. Both the blue–violet and UV emissions have excitation peaks between 5.1 and 5.2 eV and the PLE peak of the blue–violet is accompained by a very weak transition around 3.7 eV. Similar to the PL emission, the intensity of the PLE peaks increases and reaches a maximum value for the larger cluster system at 900 °C. In addition, Fig. 2 shows that the excitation energy of the spectra remains unchanged for different annealing temperatures. The most important features of the blue–violet PL emission are listed in Table I.

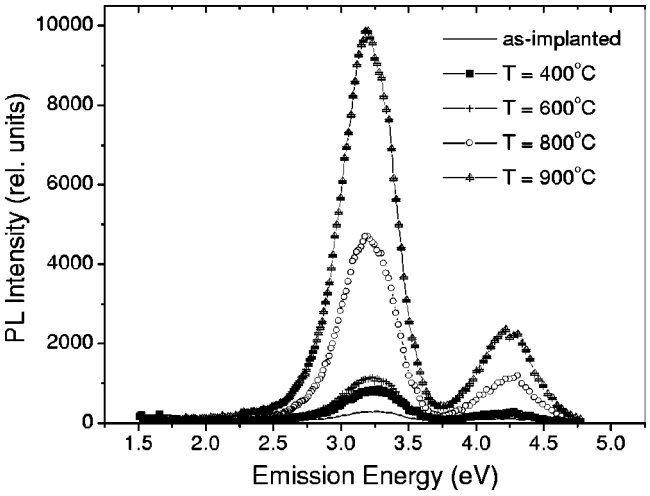

FIG. 1. PL spectra of Ge-implanted SiO_2 layers after implantation (as implanted) and at different anneal temperatures, under energy excitation of 5.17 eV.

B. Microstructure characterization

Figure 3 displays cross-sectional TEM images (underfocused) showing Ge-implanted SiO_2 layers thermally annealed at 400 [Fig. 3(a)] and 900 °C [Fig. 3(b)]. In contrast to previous observations where Ge crystalline clusters were no-

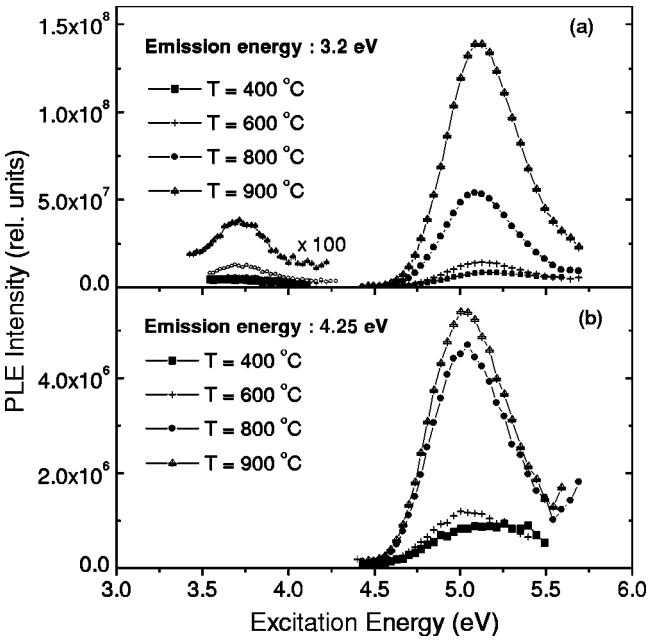

FIG. 2. PLE spectra of Ge-implanted SiO_2 layers at different anneal temperatures for blue–violet emission (a) and UV emission (b).

TABLE I. Blue–violet PL values of the Ge-nanocluster system in SiO_2 for all the annealing temperatures.

Blue–violet PL values						
Anneal temperature (°C)	PL emission intensity, I (relative units)	$I/I_{(400\,°C)}$	Emission peak position (eV)	FWHM (eV)	Excitation peak position (eV)	
400	812	1.0	3.22	0.48	~5.16;	~3.71
600	1130	1.4	3.21	0.45	~5.12;	~3.74
800	4660	5.7	3.19	0.45	5.10;	3.72
900	9760	12.0	3.19	0.44	5.11;	3.73

ticed only at higher temperatures,[14,15] clusters in the crystalline phase can even be observed at $T=400\,°C$ [see the inset in Fig. 3(a)]. At this temperature, the monomodal size distribution of nanoclusters is characterized by mean diameter $\langle\phi\rangle=2.2$ nm and standard deviation $\sigma=0.5$ nm. With an increase of the annealing temperature, the particle size distribution (PSD) evolves monotonically. At 900 °C it can be characterized by $\langle\phi\rangle=5.6$ nm and $\sigma=1.7$ nm. The $\langle\phi\rangle$ and σ values were obtained by considering populations of more than 300 particles. Concomitant with the evolution in size as a function of T, the depth distribution of the precipitate system becomes narrower and is centered in the region around the maximum of the implanted profile. We also note [see Fig. 3(b)] that smaller clusters are present at the ''wings'' of the depth distribution, while larger ones are located at the center of the distribution. With an increase of annealing temperature, the RBS measurements [see Figs. 3(a) and 3(b)] also demonstrate that the depth distribution of the Ge content becomes narrower and is centered in the region where the larger clusters formed. In addition, the RBS measurements show that the total Ge content is conserved within the SiO_2 layer. However, with an increase of temperature, a small fraction of the implanted Ge atoms tends to segregate at the SiO_2/Si interface. For the 900 °C case, the segregated amount corresponds to ≈3% of the implanted content and careful TEM observations have not detected Ge clusters in the interface region. Table II summarizes the above TEM and RBS results.

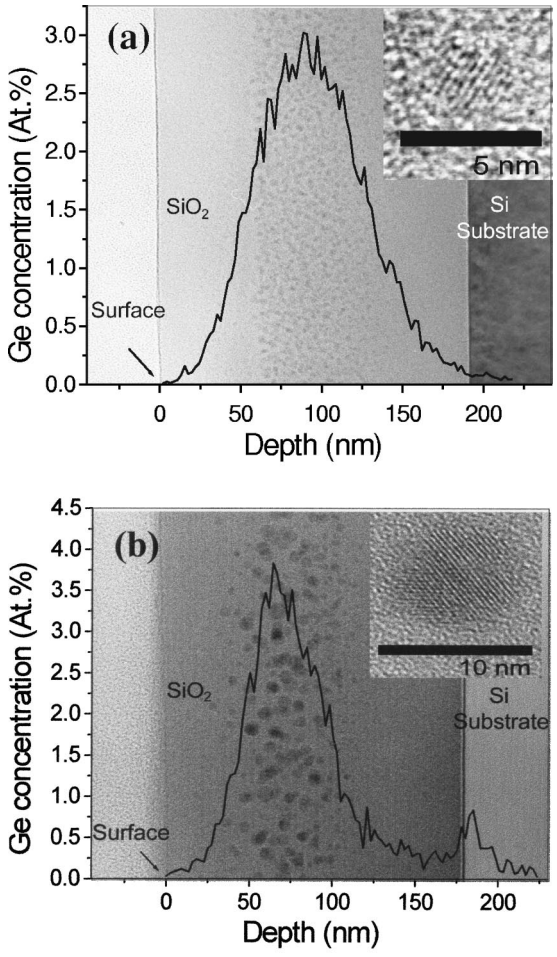

FIG. 3. Cross-sectional TEM images of Ge nanoclusters in SiO_2 layers after post-implantation annealing at 400 (a) and 900 °C (b). The insets show lattice images of the nanoclusters. The solid lines give the concentration–depth distribution of Ge obtained from RBS.

Assuming standard coarsening theory, it is expected that, concomitant with cluster growth as a function of the temperature (see Table II), exponential reduction of the Ge solute concentration should take place. In order to test this concept, we performed a detailed investigation of the Ge nanocluster/SiO_2 system via plan-view bright field (BF) TEM observations. In this geometry, we were able to determine the PSD and the total cluster concentration per unit area by directly evaluating the precipitate dimensions from the micrographs shown in Fig. 4. It is important to mention that the PSDs obtained from the plan-view samples were consistently similar to the ones obtained from cross-sectional measurements. Furthermore, by using the total Ge content determined by the RBS measurements and taking into account the density of crystalline Ge, we have estimated the fraction of Ge content trapped in the TEM observable clusters (i.e., clusters with diameter $\phi>0.8$ nm), which are plotted in Fig. 5 as a function of the annealing temperature. The Ge fraction at 400 °C could not be calculated because the high density of small Ge nanoclusters leads to superimposition of the observed cluster images in the two-dimensional projection recorded by the micrograph. For 900 °C, about 75% of the Ge atoms are trapped in clusters, and as shown by the RBS spectrum 3% of the implanted Ge atoms is redistributed outside the cluster region, and it moves towards the SiO_2/Si interface without the formation of TEM observable clusters. This means that at this temperature a rather significant fraction of about 20% of the Ge atoms is distributed in the matrix or in nanoclusters with diameters $\phi<0.8$ nm.

TABLE II. Microstructure and RBS results of the Ge-nanocluster system in SiO_2 for all the annealing temperatures. The typical error in RBS measurement is ±5%.

	Particle size distribution (TEM)		Ge depth distribution (RBS)			
Anneal temperature (°C)	Mean diameter (nm)	Standard deviation (nm)	Mean depth (nm)	Standard deviation (nm)	Ge fraction in clusters (at. %)	Total interface area (cm^2/cm^2)
400	2.2	0.5	92	33	···	0.55[a]
600	3.6	0.7	84	33	42.5	0.51
800	4.1	1.0	83	25	55	0.49
900	5.6	1.7	71	21	75	0.48

[a]This value was obtained assuming a Ge fraction in the clusters of 40 at. % estimated by extrapolation of the fitted curve in Fig. 5.

Additionally, the evolution of the total cluster–matrix interface area was studied for the present Ge–SiO_2 system. The values of the areas were obtained by considering the PSD of the Ge nanoclusters determined by cross-sectional TEM and the total cluster concentration of the region observed. However, a cluster concentration in the cross-sectional image cannot be accurately obtained due to the unknown thickness and the thickness variations over the area of observation of TEM specimens. On the other hand, taking into account the known Ge fraction incorporated into the clusters (see Table II), the Ge concentration obtained from the RBS measurements can be used to scale the proper cluster concentration. Hence, correlating this result with the PSD, we can obtain the total interface area of the observed Ge nanoclusters located within the SiO_2 layer. The results are listed in the Table II. Here, it is important to remark that, for the 400 °C case, the value was estimated by considering extrapolation of the Ge fraction in clusters provided by the fitted curve shown in Fig. 5.

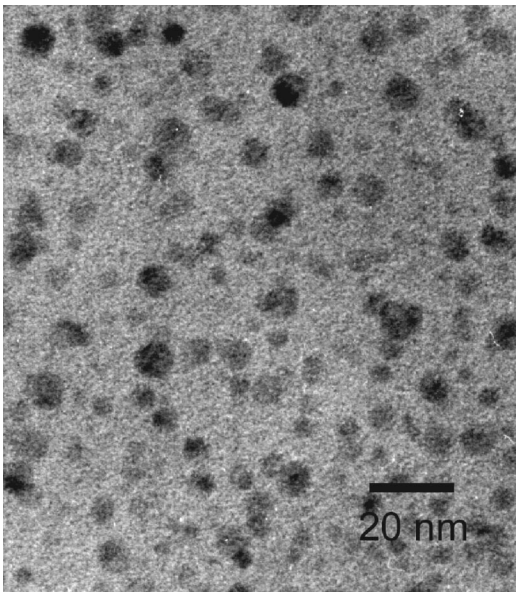

FIG. 4. Plan-view BF TEM micrograph showing Ge nanoparticles obtained after 900 °C thermal annealing for 30 min. Notice that the Ge nanoparticles are well defined and separated, allowing determination of the particle areal density.

IV. DISCUSSION

The results shown in Figs. 1 and 2 (and summarized in Table I for the blue–violet PL) reveal that the PL emission and excitation peaks remain unshifted in energy and no significant change in the FWHM is observed for different cluster mean diameters (from 2.2 to 5.6 nm) as a function of the temperature. This is in agreement with the PL data in Ref. 13 and means that one can exclude quantum confinement effects in Ge nanoclusters as a main mechanism for the origin of PL bands in the present Ge–SiO_2 system. In addition, the authors of Ref. 13 have also shown that the existence of oxygen-related defects that formed in the SiO_2 matrix as a consequence of implantation-induced radiation damage itself can be ruled out as an alternative source of luminescence in the visible and UV spectral regions since inert gas implant experiments did not produce such a large increase in the PL intensity. As a consequence, the intense PL from Ge-implanted SiO_2 layers has been heuristically attributed to the formation of ODCs in ≡Ge-Ge≡ or ≡Ge-Si≡ structures, denoted as neutral oxygen vacancies (NOVs). These molecule-like luminescence centers have a three-level energy system in which blue–violet emission (~3.2 eV) and UV emission (~4.25 eV) are due to a triplet-to-singlet transition ($T_1 \rightarrow S_0$) and a singlet-to-singlet transition ($S_1 \rightarrow S_0$), re-

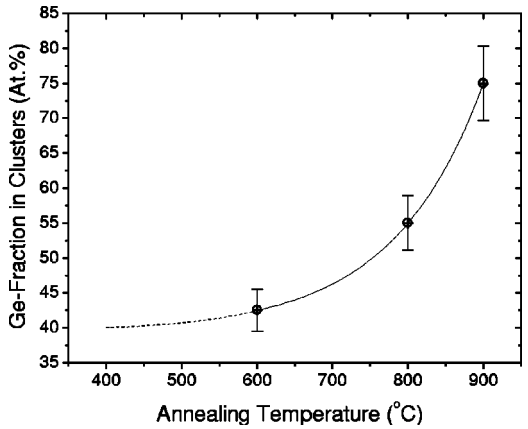

FIG. 5. Ge fraction in clusters (observed by plan-view BF TEM) as a function of the annealing temperature. The line is drawn only to guide the eyes. The error bars correspond to a combination of a 5% RBS error and an estimated 5% error from TEM observations.

spectively. As also seen previously,[13] NOVs are created in the oxide layer after postimplantation thermal treatment and may also occur at the Ge nanocluster–oxide interface for annealing at high temperatures.

Therefore, it seems reasonable to consider that the evolution of specific structural characteristics of the clusters themselves, or of their interfaces with the matrix, should play a central role related to the increase of PL intensity with the annealing temperature. The coarsening evolution shown in Fig. 3 is very similar to what is typically observed in precipitate systems produced by ion implantation.[16,17] It can be characterized as nonhomogeneous Ostwald ripening coarsening behavior driven by minimization of the system interface-free-energy. This is a consequence of the reduction of the total cluster–matrix interface area, which occurs concomitantly with cluster growth and a reduction of the solute concentration, as summarized in Table II. In the present case, we have observed that in spite of the very small reduction of total interface area (i.e., reduction of Ge atoms on the cluster surface) the PL intensity increases monotonically by a factor of 12 from 400 to 900 °C annealing temperature. Hence, in this case it seems to be rather contradictory to attribute the increase of the PL intensity directly to the creation of NOV centers formed by Ge atoms located at the cluster surface. At 400 °C, despite the observed nucleation of the Ge nanoclusters, the highest fraction, about 60%, of Ge atoms is distributed in the matrix (see Fig. 5), probably located in solution or in small clusters ($\phi < 0.8$ nm), or in the form of nonradiative paramagnetic E' centers ($\equiv$Ge•) formed during implantation. Since the PL intensity has its lower value the Ge content trapped in NOV luminescence centers seems to still be small. The results in Fig. 5 show that the expected reduction of solute concentration as a function of the temperature occurs concomitantly with cluster growth. However, at 900 °C, a rather significant fraction, about 20%, of the Ge atoms is still distributed in the matrix within the region where the cluster band formed.

Hence, in order to explain the coarsening and the PL behavior as a function of the annealing temperature, it seems necessary to consider alternative atomic processes that take place during precipitate growth in order to provide support for the NOV formation concept. First, it is obvious that the precipitate growth process takes place via the incorporation of individual Ge atoms that exist in solution. The sources of Ge atoms are the solute field and the smaller precipitates which tend to dissolve according to the Ostwald ripening concept. The diffusion process of Ge in SiO_2 has not been systematically investigated. Nevertheless, it is plausible that Ge is a rather insoluble fast diffusing element in the amorphous SiO_2 network since precipitation and significant atomic redistribution towards the depth layer containing the larger precipitates takes place. Second, it also seems plausible to assume that the precipitate growth process requires the dissolution of SiO_2 molecules and the out-diffusion of the atomic species (Si and O) in order to accommodate the volume increase of the growing precipitates. Third, on the basis of dry oxidation experiments, it has been established that O_2 molecules are fast diffusion species whereas Si atoms redistribute over a very limited range (1–2 nm) near the SiO_2/Si interface.[18] Assuming that similar behavior occurs at the Ge nanocluster/SiO_2 interfaces, the diffusion kinetics of these species can cause enrichment of Si atoms near the growing clusters concomitantly to a deficiency of oxygen, which would not allow temperature-dependent recovery of the oxide network (i.e., $\equiv$Si-O-Si$\equiv$) around the precipitates. Hence, we speculate that the Si enrichment and possible annealing of the E' centers lead to the trapping of Ge atoms present in solution and allow the formation of NOV centers in $\equiv$Ge-Si$\equiv$ or $\equiv$Ge-Ge$\equiv$ structures. Thus, in spite of the fact that at 900 °C a lower fraction of Ge atoms is present in solution, at this temperature the diffusion of the O_2 species is more pronounced and a higher number of Ge atoms are trapped in NOV centers, thus explaining the increase of the PL intensity as a function of the annealing temperature.

V. SUMMARY

In contrast to previous results for Ge-implanted SiO_2 layers, where Ge crystalline nanocrystals were observed only at higher T, our data show that crystalline clusters have already formed at an annealing of 400 °C.

Upon annealing at higher temperatures, the cluster system follows conservative (Ostwald ripening) coarsening behavior characterized by the increase of the Ge nanoparticle mean diameters from 2.2 nm at 400 °C to 5.6 nm at 900 °C. The coarsening evolution occurs concomitantly with the increase of PL intensity by a factor of 12 within the same temperature range. This PL behavior is demonstrated to be inconsistent with quantum confinement concepts or only via the formation of ODCs at the cluster–matrix interfacial region because no significant change was observed in the total cluster–matrix interface area in the same temperature range described above. Furthermore, a combination of TEM observations and RBS measurements has shown an increase of the Ge fraction in the clusters with the temperature increase. However, at the higher temperature (900 °C) a significant fraction of the implanted Ge content ($\approx$20%) is still not located in the Ge nanoparticles, but, rather, distributed around them. The dissolution of SiO_2 molecules that allows a volume increase of the growing nanoparticles, as well as the diffusion properties of the Si and O_2 species within the SiO_2 matrix is invoked to propose a model. In this model we assume that the formation of an oxygen deficient region around the nanoparticles allows temperature-dependent trapping of Ge atoms in the form of $\equiv$Ge-Ge$\equiv$ or $\equiv$Ge-Si$\equiv$ NOV structures, thus explaining the increase of PL intensity as a function of the annealing temperature.

ACKNOWLEDGMENTS

This work was partially supported by the Brazilian agencies CNPq, CAPES and FINEP. One of the authors (P.F.P.F.) also acknowledges support from the A.v.H. Foundation, Germany.

[1] L. T. Canham, Appl. Phys. Lett. **57**, 1046 (1990).
[2] E. Werva, A. A. Sephin, L. A. Chin, C. Zhou, and K. D. Kolenbrander, Appl. Phys. Lett. **64**, 1821 (1994).
[3] A. K. Dutta, Appl. Phys. Lett. **68**, 1189 (1996).

[4] F. Iacona, G. Franzó, and C. Spinella, J. Appl. Phys. **87**, 1295 (2000).
[5] G. A. Kachurin, I. E. Tyschenko, K. S. Zhuravlev, N. A. Pazdnikov, V. A. Volodin, A. K. Gutakovski, A. F. Leier, W. Skorupa, and R. A. Yankov, Semiconductors **31**, 626 (1997).
[6] M. Brongersma, A. Polman, K. S. Min, and H. A. Atwater, J. Appl. Phys. **86**, 759 (1999).
[7] T. Shimizu-Iwayama, D. E. Hole, and P. T. Townsend, Nucl. Instrum. Methods Phys. Res. B **147**, 350 (1999).
[8] B. G. Fernandez, M. López, C. García, A. Pérez-Rodríguez, J. R. Morante, C. Bonafos, M. Carrada, and A. Claverie, J. Appl. Phys. **91**, 798 (2002).
[9] L. Rebohle, J. von Borany, R. A. Yankov, W. Skorupa, I. E. Tyschenko, H. Frob, and K. Leo, Appl. Phys. Lett. **71**, 2809 (1997).
[10] T. Gao, X. M. Bao, F. Yan, and S. Tong, Phys. Lett. A **232**, 321 (1997).
[11] S. Im, J. Y. Jeong, M. S. Oh, H. B. Kim, K. H. Chae, C. N. Whang, and J. H. Song, Appl. Phys. Lett. **74**, 961 (1999).
[12] W. S. Lee, J. Y. Jeong, H. B. Kim, K. H. Chae, C. N. Whang, S. Im, and J. H. Song, Mater. Sci. Eng., B **69–70**, 474 (2000).
[13] L. Rebohle, J. von Borany, H. Frob, and W. Skorupa, Appl. Phys. B: Lasers Opt. **B70**, 131 (2000).
[14] C. Bonafos, B. Garrido, M. López, A. Pérez-Rodríguez, J. R. Morante, Y. Kihn, G. Ben Assayag, and A. Claverie, Mater. Sci. Eng., B **69–70**, 380 (2000).
[15] A. Markwitz, L. Rebohle, H. Hofmeister, and W. Skorupa, Nucl. Instrum. Methods Phys. Res. B **147**, 361 (1999).
[16] P. F. P. Fichtner, W. Jäger, K. Radermacher, and S. Mantl, Nucl. Instrum. Methods Phys. Res. B **59/60**, 632 (1991).
[17] D. A. Porter and K. E. Easterling, *Phase Transformations in Metals and Alloys* (Chapman and Hall, London, 1992).
[18] I. J. R. Baumvol, C. Krug, F. C. Stedile, F. Gorris, and W. H. Schulte, Phys. Rev. B **60**, 1492 (1999).